sustainability

MDPI

Article

Meteorological Drought Analysis in the Lower Mekong Basin Using Satellite-Based Long-Term CHIRPS Product

Hao Guo [1,2,3,4], Anming Bao [1,4,*], Tie Liu [1,4], Felix Ndayisaba [1,2,5], Daming He [6], Alishir Kurban [1,4] and Philippe De Maeyer [3,4]

1 State Key Laboratory of Desert and Oasis Ecology, Xinjiang Institute of Ecology and Geography, Chinese Academy of Sciences, Urumqi 830011, China; casguohao@163.com (H.G.); liutie@ms.xjb.ac.cn (T.L.); davfelix@yahoo.fr (F.N.); alishir@ms.xjb.ac.cn (A.K.)
2 University of Chinese Academy of Sciences, Beijing 100039, China
3 Department of Geography, Ghent University, Gent 9000, Belgium; Philippe.DeMaeyer@UGent.be
4 Sino-Belgian Joint Laboratory of Geo-information, Urumqi 830011, China and Ghent 9000, Belgium
5 University of Lay Adventists of Kigali (UNILAK), 6392 Kigali, Rwanda
6 Asian International Rivers Center, Yunnan University, Kunming 650091, China; dmhe@ynu.edu.cn
* Correspondence: baoam@ms.xjb.ac.cn; Tel.: +86-0991-788-5378

Academic Editor: Audrey Mayer
Received: 9 May 2017; Accepted: 25 May 2017; Published: 29 May 2017

Abstract: Lower Mekong Basin (LMB) experiences a recurrent drought phenomenon. However, few studies have focused on drought monitoring in this region due to lack of ground observations. The newly released Climate Hazards Group Infrared Precipitation with Station data (CHIRPS) with a long-term record and high resolution has a great potential for drought monitoring. Based on the assessment of CHIRPS for capturing precipitation and monitoring drought, this study aims to evaluate the drought condition in LMB by using satellite-based CHIRPS from January 1981 to July 2016. The Standardized Precipitation Index (SPI) at various time scales (1–12-month) is computed to identify and describe drought events. Results suggest that CHIRPS can properly capture the drought characteristics at various time scales with the best performance at three-month time scale. Based on high-resolution long-term CHIRPS, it is found that LMB experienced four severe droughts during the last three decades with the longest one in 1991–1994 for 38 months and the driest one in 2015–2016 with drought affected area up to 75.6%. Droughts tend to occur over the north and south part of LMB with higher frequency, and Mekong Delta seems to experience more long-term and extreme drought events. Severe droughts have significant impacts on vegetation condition.

Keywords: drought; SPI; CHIRPS; remote sensing; Lower Mekong Basin

1. Introduction

Drought is considered as one of the costliest and most damaging as well as one of the most complex and least understood natural hazards due to its high heterogeneity in space and variability in time [1–3]. Droughts can be broadly divided into four types: (a) meteorological; (b) agricultural; (c) hydrological; and (d) socioeconomic [2,4]. Meteorological drought occurs first as a consequence of precipitation deficit followed by agricultural and hydrological drought because all other three drought types are mainly driven by the continuous precipitation deficit [5].

SPI is the most popular and commonly used precipitation deficit index to reflect drought condition. Developed by McKee et al. [6], SPI is a simply computed drought index which is only based on long-term precipitation records. The most attractive feature of SPI is its suitability to different regions at flexible timescales [7,8]. Besides, it can also be applied to reflect flood conditions in addition to

drought monitoring [9,10]. Based on the above advantages, the World Meteorological Organization (WMO) suggests SPI as the reference drought index [11]. The SPI has been widely applied to study the characteristics of drought, such as drought forecasting [12], drought frequency analysis [13,14], spatiotemporal drought analysis [15,16], drought period and severity [17], and climate change impact studies [18]. Therefore, SPI is used in this study as the drought monitoring index.

Conventional drought monitoring depends on ground observations which have relatively high accuracy and long-term records. However, the ground-based precipitation observation networks are sparse and nonhomogeneous or not available for common users in many regions around the world such as Mekong River Basin [19]. Due to the limited and variable representativeness, drought monitoring based on ground observations is subject to limitations and drawbacks. Spatial interpolation may be one possible solution, however, it will introduce high uncertainty, especially for the mountainous regions with sparse and uneven gauges [20,21].

With the development of remote sensing technique, a variety of satellite-based precipitation retrieval algorithms have been produced by combining both Infrared (IR) and passive microwave (PMW) estimates from different sensors in recent years, such as Tropical Rainfall Measuring Mission (TRMM), Multi-satellite Precipitation Analysis (TMPA) [22], Climate Prediction Center morphing technique (CMORPH) [23], Global Satellite Mapping of Precipitation (GSMaP) [24], NRL-Blend satellite rainfall estimates from the Naval Research Laboratory (NRL) [25] and Precipitation Estimation from Remotely Sensed Information using Artificial Neural Networks (PERSIANN) [26,27]. Based on their advantages of large-scale coverage, high spatiotemporal resolution and public accessibility, satellite precipitation estimates are playing increasingly important role in providing supplemental data resources for different meteorological and hydrological applications such as flood and landslide monitoring [28–30]. Though some evaluation works have been reported for drought monitoring by using short-term satellite precipitation products, the error from the limited data record should be studied further [15,31,32] because the time series of most products are too short for confident drought monitoring, which should be based on historical data with at least 30 years length of record [33,34].

PERSIANN Climate Data Record (PERSIANN-CDR) [35] and Climate Hazards Group Infrared Precipitation with Station data (CHIRPS) [36] are two newly developed long-term satellite-based precipitation products which can meet the demand of precipitation characteristics and drought monitoring at a climate time scales for more than 30 years. The two satellite-based precipitation products with long-term records provide valuable data resources for studying the spatial and temporal characteristics of increasingly frequent droughts.

Due to their late availability, few efforts have been made to investigate the performance of PERSIANN-CDR and CHIRPS products to estimate the amount and spatial distribution of precipitation, as well as their potential for being applied in drought monitoring. Miao et al. [19] evaluated PERSIANN-CDR's performance in capturing the behavior of daily extreme precipitation events in China from 1983 to 2016 and found that the performance of PERSIANN-CDR is good in most parts of China. Based on gridded gauge dataset, the performance of PERSIANN-CDR for monitoring meteorological drought events was also evaluated from 1983 to 2014 over Mainland China. It was found that PERSIANN-CDR showed reasonable performance for drought monitoring over most of China [17]. In comparison to a dense and reliable gauge network from 1981 to 2010, CHIRPS showed good correlation over Cyprus [37] and CHIRPS also gave a promising performance in capturing precipitation extremes [38]. When applied as input precipitation information in streamflow simulation in Italy, CHIRPS also suggested satisfactory performance [39]. However, little has been done to evaluate the performance and the possibility for application of CHIRPS data in drought monitoring. While contrasting PERSIANN-CDR and CHIRPS for drought monitoring over Chile, it was found that CHIRPS had a better fit with in-situ observations than PERSIANN-CDR and were more applicable for regional drought monitoring with higher spatial resolution (0.05°) and longer periods of data records (36 years till now) [40].

The Mekong River basin is one of the most important transboundary river basins in Southeast Asia [41]. Over the last decades, LMB has experienced frequent drought events. For example, severe drought events occurred during 1992–1993, 1998–1999, 2003–2005 and 2010–2011 [42–44]. The worst drought in decades occurred beginning from late 2015 and continued through July 2016, with impacts spread over Vietnam, Cambodia, Laos and Thailand. These droughts have great impacts on the local agriculture, forestry, water resources, industry, and the environment [44]. Therefore, drought monitoring in LMB is of primary necessity for water planning and management to mitigate their detrimental impacts on the society, economy and environment. However, the ground-based precipitation gauges are very limited or unavailable for common users.

In this study, the performance of CHIRPS for precipitation capturing and drought monitoring is firstly evaluated through a direct quantitative comparison based on ground observations and an indirect comparison by using surface soil moisture (SM). Based on long-term CHIRPS product and SPI drought index, the primary objective of this study is to describe the spatiotemporal characteristics of meteorological droughts in LMB at multiple time scales. In addition, the drought impacts on vegetation are also analyzed. This is one early study to assess and apply CHIRPS for drought monitoring over Lower Mekong Basin, spanning the time from January 1981 to July 2016. The results of this paper will provide useful insights on the stability of CHIRPS for drought monitoring and contribute to a more comprehensive understanding of historical droughts over LMB, which are very important for the water resources management and design of contingency plans to reduce the impacts of droughts.

2. Study Region, Datasets and Methods

2.1. Study Area

As the 12th longest river in the world and longest river in South Asia, Mekong River has a length of 4880 km [43,45]. The Lower Mekong Basin (LMB) is the downstream part of Mekong River Basin, which encompasses parts of four countries: Laos, Thailand, Cambodia, and Vietnam (Figure 1a). This region covers approximately 618,783 km^2 with forest and agricultural land accounting to nearly 35% and 40%, respectively. The topography of the LMB is mainly organized by the Northern Highlands, Khorat Plateau, Tonle Sap Basin, and Mekong Delta (Figure 1b) from north to south. Plains (lower than 200 m) mainly limited in Thailand, Cambodia, and Vietnamese Mekong Delta and high mountains located mostly in Laos are the two main terrain feathers [42]. The LMB is a tropical monsoon region with a monthly mean temperature of 20 °C and annual accumulated precipitation of about 1000 mm. This area experiences two distinctly different seasons: the wet summer season from May to October influenced by the moist Southwest Monsoon and the dry winter season from November to the April influenced by the dry Northeast Monsoon [46].

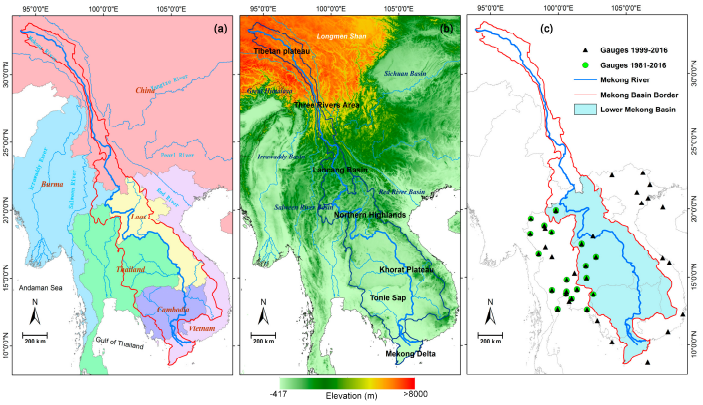

Figure 1. Maps of the Mekong Basin: (**a**) river network; (**b**) topography; and (**c**) two group gauges based on the availability of observations (20 gauges for January 1981–July 2016 and 38 gauges for January 1999–July 2016) in the Lower Mekong Basin.

2.2. Datasets

2.2.1. The Observed Precipitation Gauge

For validating CHIRPS product, the precipitation observed records were obtained from the Global Summary of the Day (GSOD) which is released by the National Oceanic and Atmospheric Administration's (NOAA's) National Climatic Data Center (NCDC) [47]. In order to ensure a high quality of gauges, a systematic quality control procedure was carried out based on several criteria: Firstly, a filtering method was used to select the gauges with least missing data. The gauges with more than 30% missing values of time series records were not considered. In addition, rain gauges were removed when the negative values were found or daily rainfall values were larger than twice the annual average value [48]. Finally, the Normal Ratio Method [49] is applied to fill the left missing values for each selected gauge by using the two or three closest gauges.

Due to data availability limitations and for reasons relating to data quality issues, the precipitation gauge data are not limited to the scope of LMB. To ensure the data length requirement (>30 years) of computing SPI [34] and the quality of validation for CHIRPS, the gauges after quality control are divided into two groups: the first group includes 38 gauges marked with black triangles in Figure 1c with the period from January 1999 to July 2016. It is mainly used to check the performance of CHIRPS in capturing the behaviors of monthly precipitation. The second group includes 20 gauges marked with green circles in Figure 1c (from January 1981 to July 2016), whose length of the records is the same as CHIRPS'. It is applied to identify the possible error of CHIRPS for drought monitoring.

2.2.2. CHIRPS Satellite Precipitation Dataset

Developed by the U.S. Geological Survey (USGS) and the Climate Hazards Group at the University of California, Santa Barbara, CHIRPS [50] is a new land-only IR-based climatic precipitation data with high spatial resolution ($0.05^\circ \times 0.05^\circ$) and long-term records (1981-present). Global climatology, satellite estimates and gauge observations are integrated into this datasets. CHIRPS has a relatively high resolution (0.05°) than other satellite-based precipitation products which commonly have a spatial resolution of 0.25° or 0.1°. Three different temporal resolutions, pentadal, decadal, and monthly, are available online from 1981 to near-present. Here, the monthly CHIRPS version 2.0 from January 1981 to July 2016 is used, and CHIRPS version 2.0 was referred to as CHIRPS in this study for brevity.

2.2.3. AVHRR Vegetation Health Product

In order to analyze the impacts of meteorological drought on vegetation, the Vegetation Health Index (VHI) dataset collected from Advanced Very High Resolution Radiometer (AVHRR) imagery is also used in this paper. It is released by the NOAA Center online [51]. The VHI dataset has been widely applied for early drought warning, monitoring of crop yield and production and assessment of irrigated areas and excessive wetness [52–56]. VHI is a weighted average of two sub-indices: the Vegetation Condition Index (VCI) calculated from Normalized Difference Vegetation Index (NDVI) and the Temperature Condition Index (TCI) computed from brightness temperature (TB) data. Both VCI and TCI are based on AVHRR data and are averaged with uniform weighting to form the empirical VHI, which can reflect both vegetation cover and temperature anomalies [55]. The weekly VHI product with 4 km spatial resolution in GEO-TIFF format is used in this study for the period 1981 (Week 35)–2016 (Week 37). In order to check the possible impact of drought on vegetation, the weekly VHI is integrated into monthly, and the standardized anomalies index (SAI) is applied to the weekly VHI as Equation (1).

$$SAI\_VHI = \frac{VHI_i - \overline{VHI}}{\sigma_{VHI}} \quad (1)$$

where *SAI_VHI* represents the *VHI* anomalies, and $\overline{VHI}$ and σ_{VHI} are the average value and standard deviation of the *VHI* series, respectively.

2.2.4. Soil Moisture Dataset

The soil moisture dataset (SM) from the Noah model of Global Land Data Assimilation System (GLDAS) is used to cross-validate the accuracy of CHIRPS for drought monitoring. The 0–10 cm soil moisture product from 2000 to 2016 at monthly -0.25° resolution is used in this study. The soil moisture dataset is obtained from the Goddard Earth Sciences Data and Information Services Center (GES DISC) [57]. Similar to VHI, the SAI of SM is also calculated according to Equation (2).

$$SAI\_SM = \frac{SM_i - \overline{SM}}{\sigma_{SM}} \quad (2)$$

where SAI_SM means SM anomaly series, and $\overline{SM}$ and σ_{SM} are the average value and standard deviation of the SM series, respectively.

2.3. Methods

2.3.1. Statistical Evaluation Metrics

Several traditional statistical metrics, including Relative bias (RB), Pearson linear correlation coefficient (CC) and root mean square error (RMSE), are used for the validation of CHIRPS. Fractional RMSE (FRMSE) is also adopted in this study to avoid the possible rainfall volume dependent errors. The equations and optimal values of RB, CC, RMSE and FRMSE are given in Table 1.

Table 1. List of the traditional metrics used in validation of CHIRPS product.

Statistical Metric	Equation	Optimal Value
Relative Bias (RB) [1]	$RB = \sum_{i=1}^{N} (S_i - G_i) / \sum_{i=1}^{N} (G_i)$	0
Pearson linear correlation coefficient (CC) [1]	$CC = (\sum_{i=1}^{N} (S_i - \overline{S})(\mathrm{G}_i - \overline{G})) / (\sqrt{\sum_{i=1}^{N} (S_i - \overline{S})^2} \sqrt{\sum_{i=1}^{N} (G_i - \overline{G})^2})$	1
Root Mean Square Error (RMSE) [1]	$RMSE = \sqrt{\frac{1}{N} \sum_{i=1}^{N} (\mathrm{S}_i - \mathrm{G}_i)^2}$	0
Fractional RMSE (FRMSE) [1]	$FRMSE = \sqrt{\frac{1}{N} \sum_{i=1}^{N} (\mathrm{S}_i - \mathrm{G}_i)^2} / \overline{G}$	0

[1] S stands for satellite-based CHIRPS product and G represents the gauge observations. RB, CC and FRMSE are dimensionless, and RMSE is in mm/month.

2.3.2. The Standardized Precipitation Index (SPI)

Developed by McKee et al. [6], the Standardized Precipitation Index (SPI) is developed to describe precipitation deficit to reflect meteorological drought condition. Robust SPI computation should be based on long-term precipitation records (>30 years) which is accumulated over a specified timescale [58]. Generally, precipitation is on non-normal stable distribution, the long-term precipitation records are firstly fitted to a gamma distribution and then the normal distribution is transformed into a Gaussian distribution by using equal probability transformation. The most attractive feature of SPI is that drought and flood conditions can be directly compared in different regions over flexible timescales [59]. In the present paper, one-month, three-month, six-month and 12-month time scales (SPI1, SPI3, SPI6 and SPI12) are chosen to represent short- and long-term droughts. Although SPI is a kind of meteorological drought index, SPI different timescales can also be used to reflect the different drought conditions like agricultural and hydrological drought conditions [60]. The range of SPI scope is from -3 to $+3$. The positive and negative values indicate wet and dry conditions, respectively. Specific drought classifications based on SPI values are given in Table 2. In this study, the latest SPI program (SPI_SL_6) from the National Drought Mitigation Centre [61] is used to compute SPI for each gauge and grid over LMB through 427 months (more than 36 years) at different time scales.

Table 2. Drought classification according to SPI values [6].

SPI Value	Category
2.0 and above	Extremely wet
1.5 to 1.99	Severely wet
1.0 to 1.49	Moderately wet
−0.99 to 0.99	Near normal
−1.0 to −1.49	Moderately dry
−1.5 to −1.99	Severely dry
−2.0 and less	Extremely dry

2.3.3. Drought Identification and Characteristics

According to McKee et al. [6], a drought event is defined as a period when SPI is continuously below 0 with the lowest SPI value less than −1.0. Only the droughts persistent at least continuous two months are considered. Once drought events are identified, the drought indicators can be calculated by run theory (Figure 2) [62]. These indicators include drought duration (DD), drought intensity (DI), drought severity (DS) and drought area (DA). DD is the number of months in which SPI values are negative for a drought event [63]. The absolute sum of all SPI values during a drought event is regarded as drought severity (DS) and DA is defined as the area percentage between maximum drought area and total study area. DS is calculated as follows:

$$DS = \left| \sum_{i=1}^{DD} SPI_i \right| \tag{3}$$

where i is a month; SPI_i is the SPI value in month i; and DD and DS are the duration and severity of a drought event, respectively.

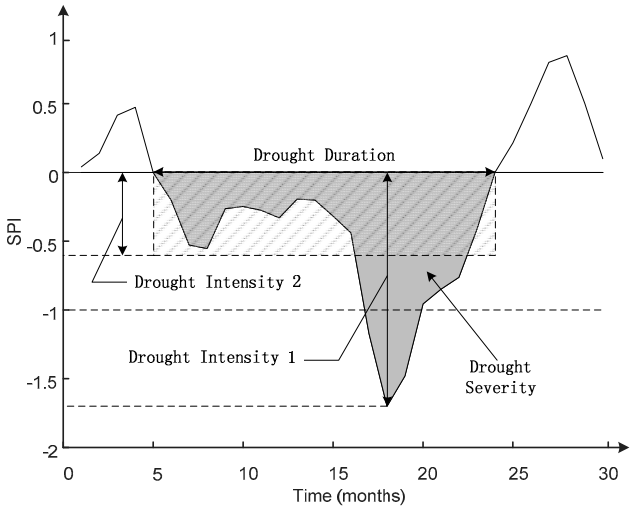

Figure 2. The run theory map of drought event and drought characteristics for drought duration (DD), drought intensity (DI1 and DI2) and drought severity (DS).

DI has two kinds of definition: the lowest SPI value [63] and severity divided by duration during the drought period [64]. Both drought intensities are adopted as DI1 and DI2 in this paper. The larger of DIs are, the more severe the drought. In addition, the total drought duration (TDD) expressed by drought month number with SPI value less than −1 through the study period is also used to assess the drought vulnerability.

3. Results

3.1. Evaluation of CHIRPS Using Rain Gauges

The satellite products should be validated before being applied in drought monitoring because the drought monitoring may be affected by their potential errors. In this section, CHIRPS product is evaluated by using selected rain gauges and gridded surface soil moisture to shed light on the capability of CHIRPS in drought monitoring.

3.1.1. Precipitation Comparison

Figure 3 gives the annual cycle of monthly precipitation and annual scatter plots based on 38 gauges from 1999 to 2016 (Figure 1c). CHIRPS performs well in capturing the annual monthly precipitation cycle in conformity with the gauge observations. However, CHIRPS seems to overestimate monthly precipitation in the rainy season and a slight underestimation is found during the dry season. The scatter plot of monthly mean precipitation for the whole year suggests that CHIRPS has an excellent agreement with observations: the scatter points are close to the 1:1 line with high CC (0.98), and low positive RB (2.68%), RMSE (12.31 mm/month) and FRMSE (0.09) (Figure 2b). The same high CC values (0.98) are also found in both dry and rainy season. The slight overestimation in the rainy season and underestimation in the dry season with low RB values (4.26% and −4.18%, respectively) exhibit consistency with the comparison of annual monthly precipitation in Figure 2a. The low FRMSE value (0.10) in rainy season indicates that the relatively high RMSE is caused by the high rainfall volume. Seasonally, CHIRPS has a better performance in the rainy season than that in the dry season with higher CC values and lower FRMSE values for most gauges. This may be related to the common season-dependent errors that satellite sensors perform well in detecting strong and convective rainfall events, but show difficulty in identifying shallow and warm rainfall events [65,66], because the CHIRPS algorithm incorporates different satellite estimates (e.g., TRMM 3B42) and depends on 0.25° TRMM training data. Generally, CHIRPS gives outstanding performance in capturing monthly rainfall compared with in-situ observations over LMB and its surrounding areas.

3.1.2. SPI Comparison

To further validate the suitability of CHIRPS for drought monitoring applications, the domain-averaged time series SPIs at different timescales (one-month, three-month, six-month and 12-month) have been calculated for the period from January 1981 to July 2016 (Figure 4). Because one needs at least 30 years of monthly values for robust SPI computation, only 20 gauges with monthly records more than 30 years are included for robust SPI calculation in this section (Figure 1c). It should be mentioned here that the SPI values shown in Figure 4 are suppressed by the spatial averaging process, while, in fact, the spatially distributed SPI values may be as low as −3 in some individual grids during drought period. In addition, the results of this part are limited to gauge stations, most of which is outside the LMB area. In other words, the SPI comparison has been employed as a proxy to assess the accuracy of CHIRPS for drought monitoring but does not reflect the drought conditions over the LMB.

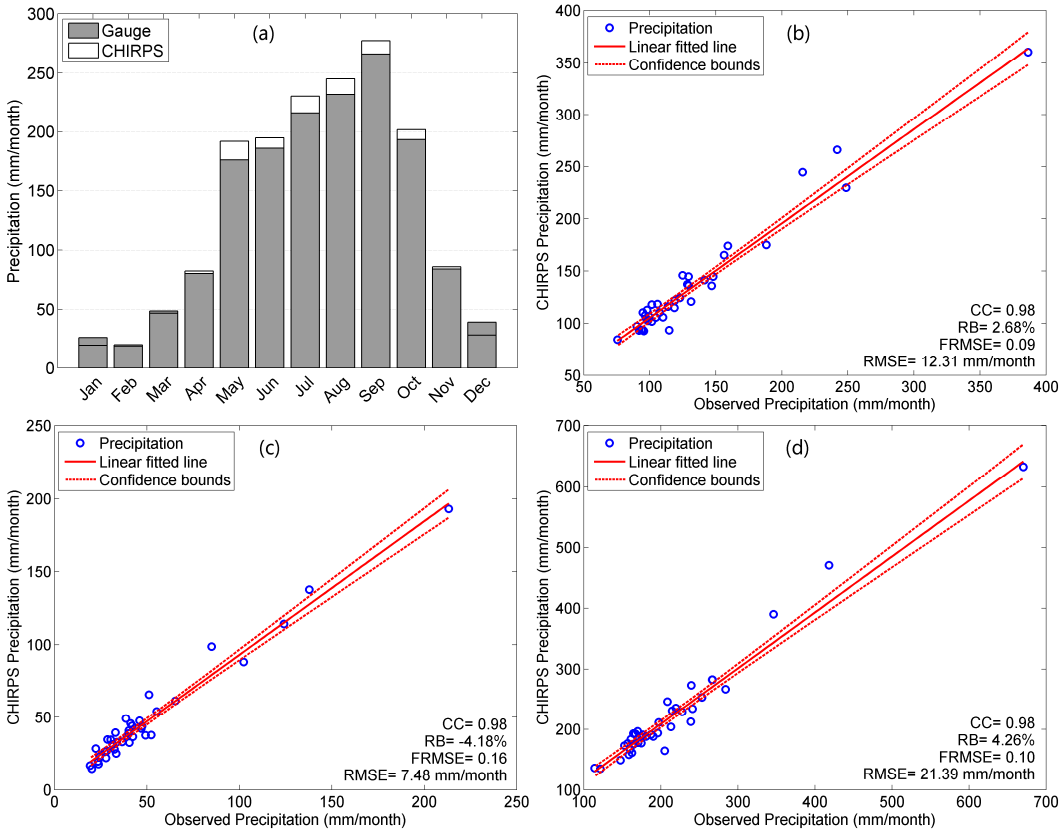

Figure 3. (**a**) Annual cycle of monthly precipitation and annual precipitation scatter plots with fitted linear line and confidence bounds of 95% based on precipitation derived from 38 gauges and corresponding grids of CHIRPS from 1999 to 2016. (**b**–**d**) Scatter plots of monthly mean precipitation for: (**b**) the whole year; (**c**) the dry season (November to April); and (**d**) the rainy season (May to October).

As can be observed in Figure 4, CHIRPS performs well in capturing the time-series SPI pattern and shows good consistency in both frequency and intensity with the gauge-derived SPIs. CHIRPS based SPI can capture drought tendencies and characteristics of drought variation at different time scales. The CCs between SPIs of CHIRPS and gauges for all time scales are higher than 0.85 and RMSEs are lower than 0.4. According to the statistics (CC and RMSE), CHIRPS and rain gauge SPIs exhibit better agreements at both three-month and six-month time scales (SPI3 and SPI6) with higher CC (0.89) and lower RMSE (0.34 and 0.35, respectively), while SPIs at 12-month time scale exhibit less agreement in terms of the lower CC (0.85) and higher RMSE (0.39). The amplitude of fluctuations for SPIs derived from CHIRPS is slightly larger than that from gauges, which indicates that CHIRPS tends to overestimate severity for both flood periods and drought periods. This phenomenon can be more easily interpreted from the comparison at longer time scales (Figure 4c,d). However, CHIRPS based SPIs seem to underestimate the drought severity during 2001–2003 at six-month and 12-month scales.

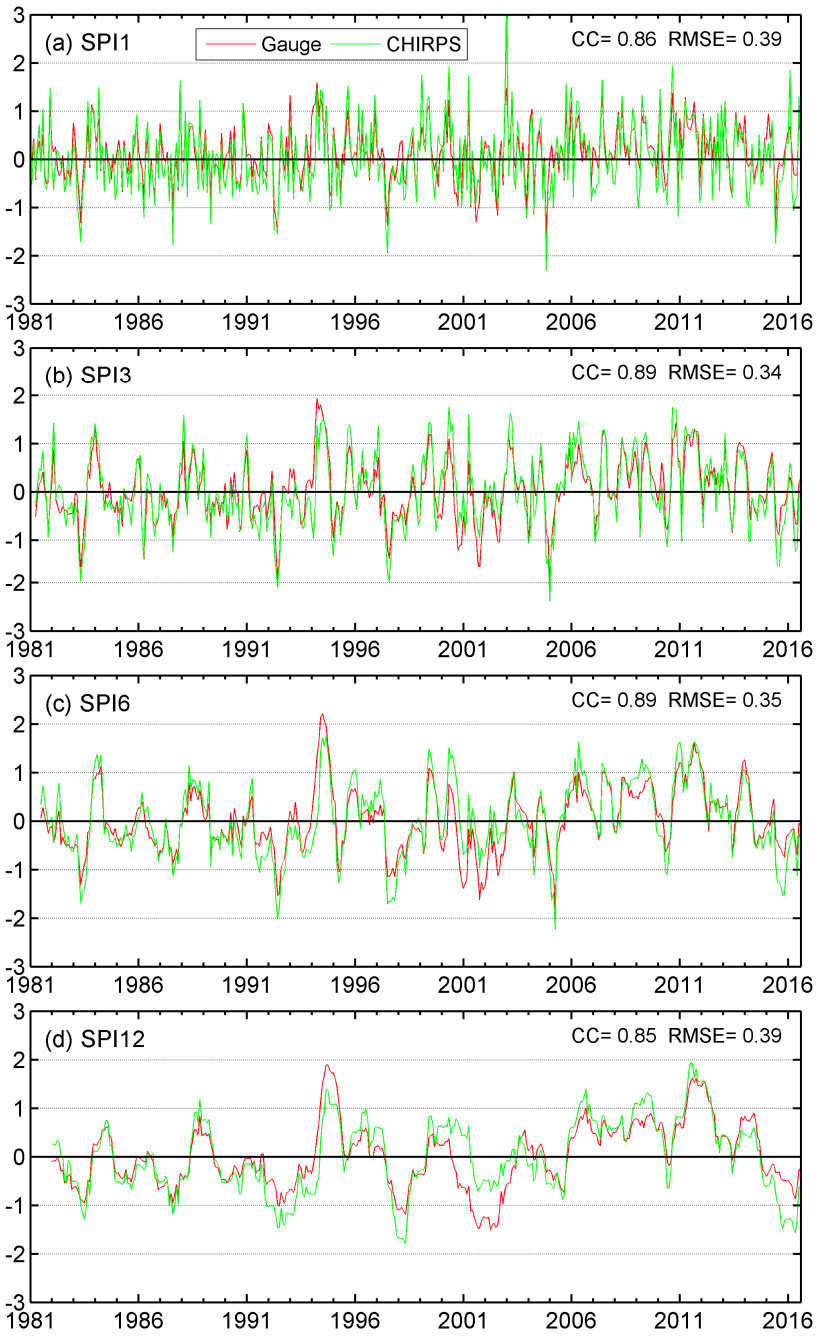

Figure 4. Spatial averaged time series SPIs for CHIRPS and rain gauges from 1981 to July 2016 at different time scales: (**a**) one-month; (**b**) three-month; (**c**) six-month; and (**d**) 12-month.

3.1.3. Cross Validation of CHIRPS

Given the fact that surface soil moisture is sensitive to drought condition, one indirect cross validation is proposed using GLDAS soil moisture dataset (0–10 cm). Here, the three-month SPI (SPI3) is used, knowing in advance that surface moisture is sensitive to short-term droughts. The spatial averaged SAI_SM and SPI3 are compared in Figure 5. Due to the availability of GLDAS SM data, the comparison is during 2000–2016 and the 2015–2016 drought event is marked by scattered rectangle.

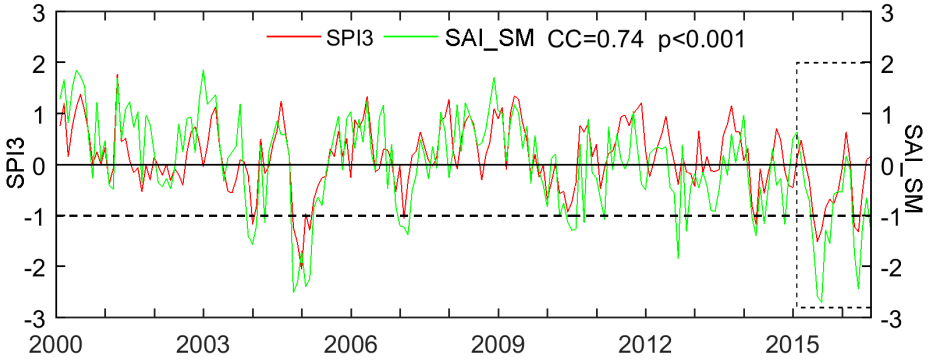

Figure 5. Time series spatial averaged SPI and SAI_SM from 2000 to 2016. The typical drought event is marked by scattered rectangle.

As can be seen that the SPI3 remains in good agreement with SAI_SM with CC as high as 0.74. The variation of SPI3 is almost identical for the variation of SAI_SM with values lower than 0 for drought periods and positive values for wet periods. For the severe drought events at three-month time scale during 2000–2016, such as the short-term drought in 2005 and drought event 4 occurring during 2015–2016 (marked by a rectangle), both SPI3 and SAI_SM are below to the normal and the drought evolutions are also similar. For instance, the drought double-peak shape is well captured by both SPI3 and SAI_SM at the same time with similar evolution shape during the 2015–2016 drought event. The results suggest that CHIRPS could effectively capture the drought events and drought evolution.

3.2. Drought Monitoring Based on CHIRPS

3.2.1. Temporal Analysis

To suggest the temporal evolution of droughts, the Hovmöller diagram was generated to provide a visualization of the temporal evolution of the SPI calculated at time scales from 1- to 12-month for the LMB (Figure 6). A drought episode is assumed as being a number of consecutive months in which the SPI values remain less than −1. It should be noted that these SPI values can only represent the average conditions at LMB scale, so higher or lower values may be found in individual grids at smaller spatial scale. These values are hard to observe because the time series SPI values are aggregated to LMB scale. The results show that drought episodes are frequent in LMB. The main persistent drought episodes identified are 1983, 1991–1994, 1998–1999, 2005 and 2015–2016, while the continuous wet periods are during 1999–2001, 2007–2010 and 2011–2013. The longest drought is identified for the period of 1991–1994. There is one short-term but severe drought in 2005, and the drought for 2015–2016 seems to be the severest one in terms of drought intensity.

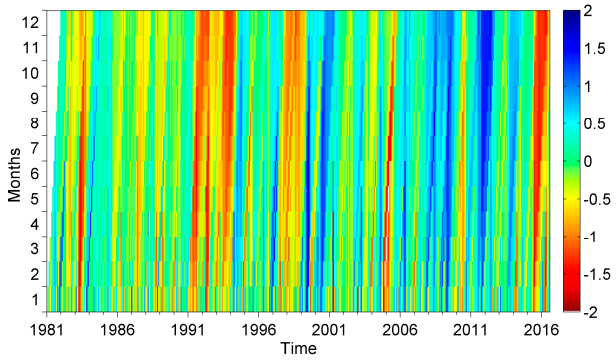

Figure 6. The Hovmöller diagram of SPI based on CHIRPS from 1- to 12-month time scales for the period of 1981–July 2016 over LMB.

Figure 7 shows the temporal evolution of SPI based on all grids over LMB, and the positive blue area and the negative red area represent the wet and dry periods based on average monthly SPI. As the time scale increases, the amplitude of SPI values and the frequency of temporal variability in time series decrease. Basically, SPI values at shorter time scales can provide early warning of drought and help to evaluate drought intensity with the lowest SPI values (DI1). In Figure 6a, there is a strong temporal fluctuation for SPI1 with alternating periods of dryness and wetness. Because SPI1 reflects short period drought conditions and its application is mainly related to meteorological drought along with short-term soil moisture and crop stress [34]. As the time scale increases and reaches cumulative durations of 12 months (Figure 7d), the separation between continuing dryness and wetness becomes much more evident, which can have a good indication of a long-term drought period.

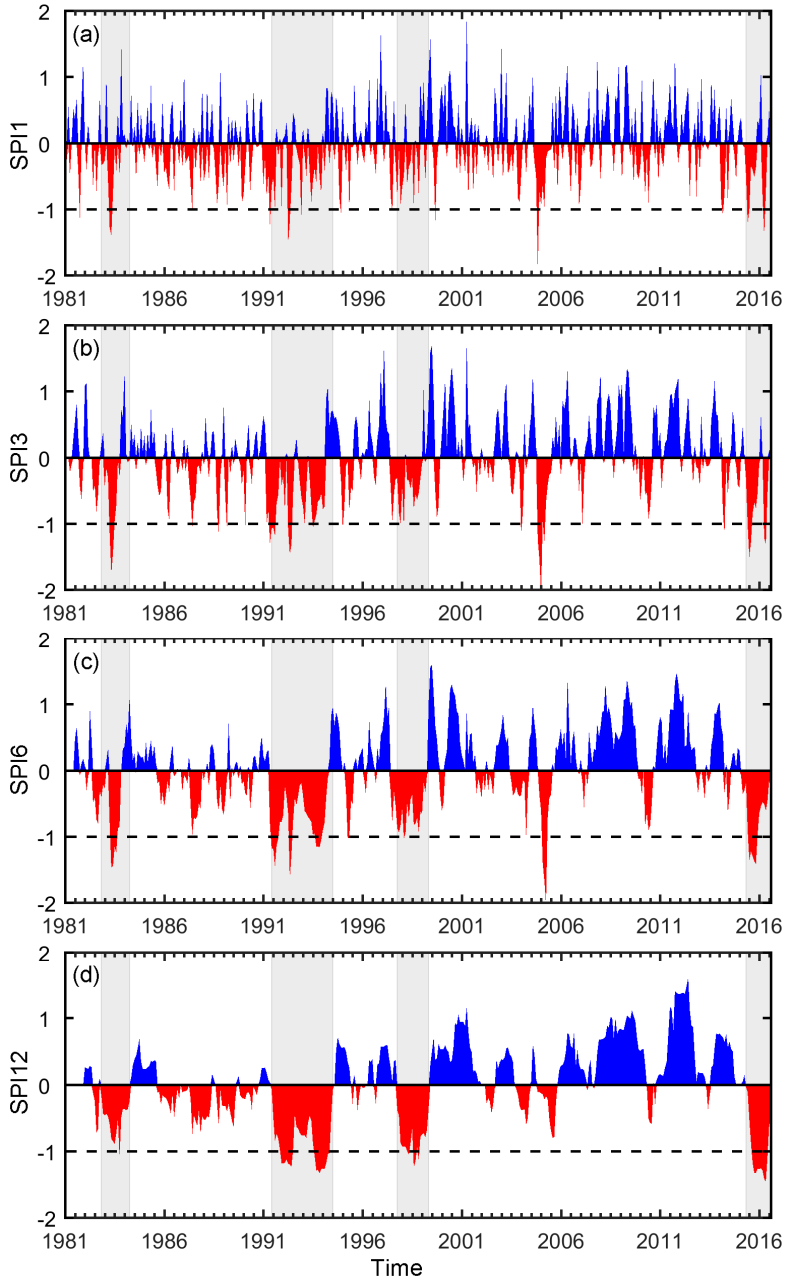

Figure 7. The temporal evolution of SPI values at different time scales: (**a**) one-month; (**b**) three-month; (**c**) six-month; and (**d**) 12-month. The gray columns highlighted in different plots represent the four most severe drought listed in Table 3.

There are fewer drought events detected during the period after 2000 than that for the period before 2000. It is noted that the drought in 2005 was quite short but severe with large negative SPI values for the short time scale. However, the SPI values at 12-month time scale are much smaller. Because SPI values at longer time scales are accumulated from SPI values at a shorter duration, which could be negative or positive, the SPIs values at longer time scales tend to lean to zero, except when an extraordinary drought or flood takes place. The drought events detected in this part are consistent with the drought period shown in Figure 6. Moreover, the results of SPI values over LMB are also in accordance with those of SPI values based on gauges, which can indirectly prove the confidence of CHIRPS for drought monitoring over LMB.

The time series of spatially distributed SPI values can be applied to evaluate the land fraction for regions under drought conditions [15]. Figure 8 displays the temporal variability of area percentage affected by moderate drought (areas in yellow), severe drought (areas in red), and extreme drought (areas in dark red) for different time scales (1-, 3-, 6-, and 12-month).

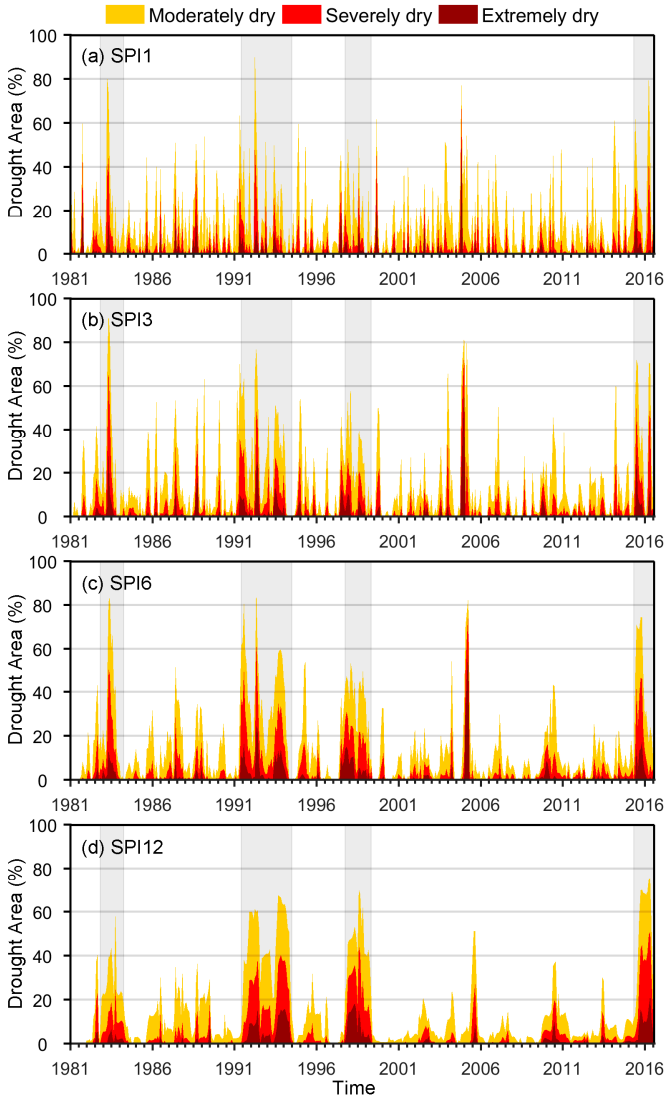

Figure 8. The temporal evolution of drought area at different time scales: (**a**) one-month; (**b**) three-month; (**c**) six-month; and (**d**) 12-month. The Orange, vermillion and red colors indicate moderate, severe and extreme dry area ratio, respectively. The gray columns highlighted in different plots represent the four most severe droughts.

The monthly SPI12 values during the study period were used to define drought events according to the definition of drought described in Section 2.3.2. LMB experienced four most severe droughts since 1981, which are listed in Table 3 with start and end time, drought duration (DD), drought severity (DS), and three drought intensity indexes (lowest SPI value, DI1; averaged DS, the maximum ratio of drought affected area, DI3). The gray rectangles in different plots in Figures 7 and 8 represent the four selected drought events listed in Table 3. The maximum drought area of these four drought events can cover up to more than 60%, which can also be seen in Figure 8.

Table 3. Characteristics of four most severe drought events at 12-month time scale over LMB.

Index	Start-End	DD	DS	DI1	DI2	DA (%)
D1	October 1982–March 1984	18	9.62	1.09	0.53	61.5
D2	May 1991–June 1994	38	33.61	1.33	0.88	67.5
D3	September 1997–April 1999	20	16.55	1.23	0.83	67.9
D4	April 2015–July 2016	16	15.50	1.45	0.97	75.6

According to drought duration (DD) and drought severity (DS), the 1991–1994 drought is the longest drought event for a drought period of 38 months with largest drought severity (33.61). While the drought in 2015–2016 is the most severe drought with lowest SPI value (−1.45) and the maximum drought affected area of 75.6%.

3.2.2. Total Drought Duration Analysis

In this study, the spatial distributed total drought duration at various time scales are adopted to study the drought occurrences with different intensity in LMB. The aim of this part is to identify regions susceptible to drought at different time scales based on the drought month number. When SPI is calculated at short time scales in areas with low seasonal precipitation, it could misleadingly lead to large positive or negative values [34,67] and LMB has quite low precipitation in the dry season (Figure 2a). Therefore, one-month SPI (SPI1) is ignored to avoid the possible misleading interpretation and the spatial distributions of SPI3, SPI6, and SPI12 are analyzed henceforth. Figure 9 gives the spatial distribution of drought month number for different drought categories (i.e., total, moderate, severe and extreme) at three timescales (3-, 6-, and 12-month).

The spatial distribution of TDD indicates that droughts tend to occur in the northern highlands and southern Tonle Sap with a TDD value greater than 80 at three-month time scale, while the most parts of central Knorat Plateau are characterized by lower frequencies (<60) (Figure 9a,e,i). As the time scale increases to longer time scales (six-month and 12-month), no major changes are observed in most parts of LMB, rather there is an increased frequency of droughts over southeastern LMB. The TDDs of moderate drought account for the majority of total droughts, and they occurred more frequently over the northern and southern parts of LMB. For 3-, 6-, and 12-month time scales, the patterns of TDD are similar except for the reduction of TDD in the north part of LMB (i.e., north highlands) when studied at longer time scales. The TDD of severe drought account for about one-quarter of TDD for droughts and has similar spatial distribution for different time scales. However, the TDDs of extreme drought have a quite distinctive spatial pattern at varying time scales. It is noted that extreme droughts are more typical in Mekong Delta region for 12-month time scales. As the time scale increases, the TDD of extreme drought in central LMB and Mekong Delta region increases as well. The southeastern part of LMB has relatively small TDD of extreme drought.

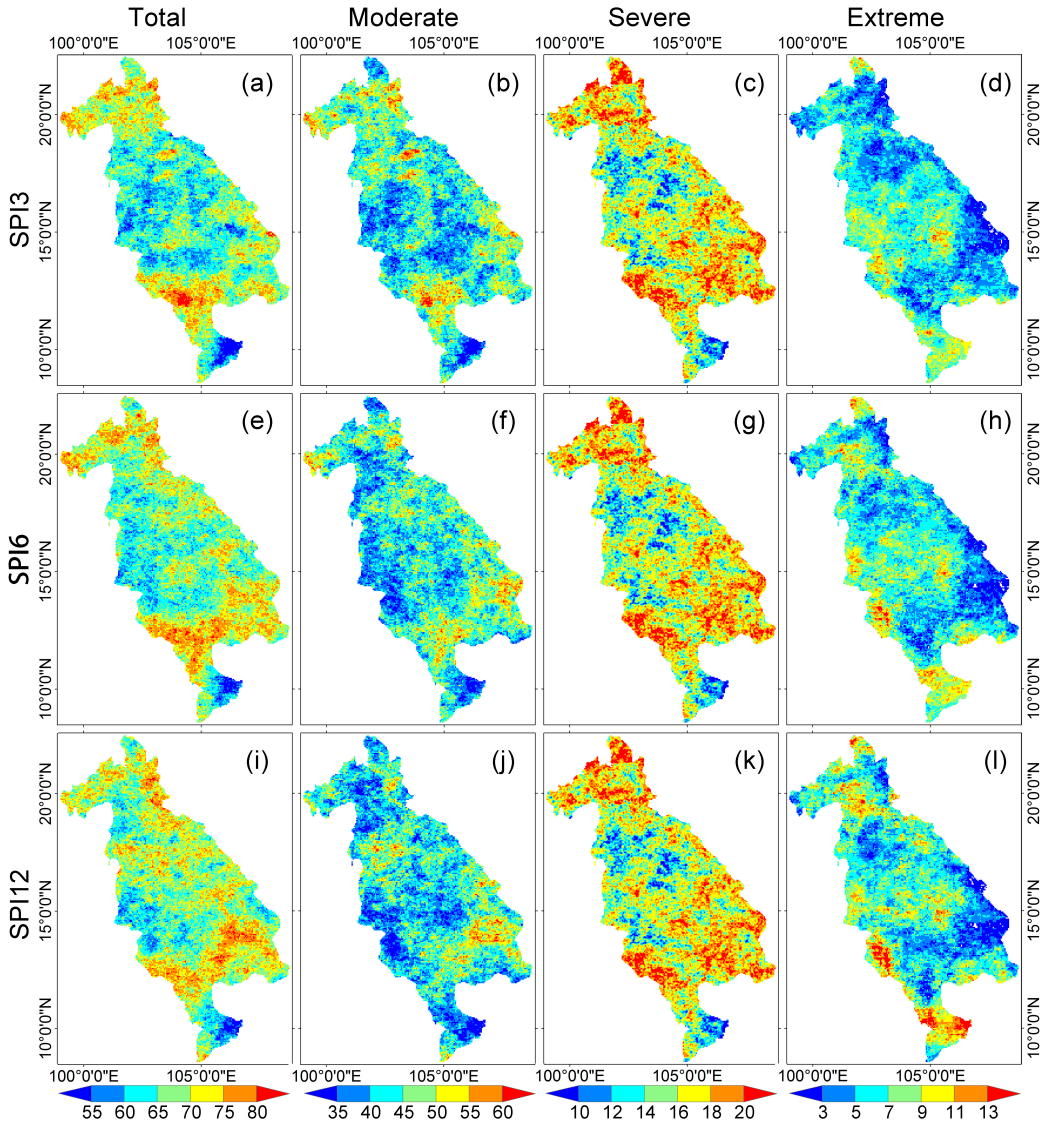

Figure 9. Spatial distribution of total drought duration (TDD) at different time scales: (**a**–**d**) three-month; (**e**–**h**) six-month; and (**i**–**l**) 12-month for different drought severities: TDD of all droughts (SPI < −1), TDD of moderate drought (−1.5 < SPI < −1), TDD of severe drought (−2 < SPI < −1.5), and TDD of extreme drought (SPI < −2) from January 1981 to July 2016.

3.2.3. Specific Drought Events Analysis

As it is widely acknowledged, the spatial distribution is critical to understand the drought events [68]. CHIRPS has a relatively higher spatial resolution which can provide more detail spatial distributions. Spatial distributions of drought indicators (i.e., DS, DI1, DI2, and max DA) for the four severest drought events listed in Table 3 are shown in Figure 10.

The four droughts have different spatial characteristics. The severity of D1 is the smallest (Figure 10a), and it mainly is restricted to the eastern part of LMB, especially for the northeast and southeast with relatively high drought intensity. The maximum DA (61.5%) is also the smallest among four drought events. It is obvious that the D2 drought is the severest drought according to the high DS values covering most parts of LMB except the Delta region (Figure 10e–h). The large value of DS is mainly attributed to the longer drought duration. The value of DI1 is quite different from DI2 although the patterns of them are similar. With respect to D3, the drought severity, as well as drought intensity for both DI1 and DI2, mainly focused on the Mekong Delta region with high DS values. According to

the values of DS and DIs, the Mekong Delta region was greatly affected by the drought that occurred from 1997 to 1999. The latest drought event occurred from late 2015 to 2016 (D4). It seems that the drought severity of this event was high, while drought duration was relatively short compared to the three other events. However, D4 is the most intense drought event with high values of DI1 and DI2, as well as the highest maximum DA up to 75.6%.

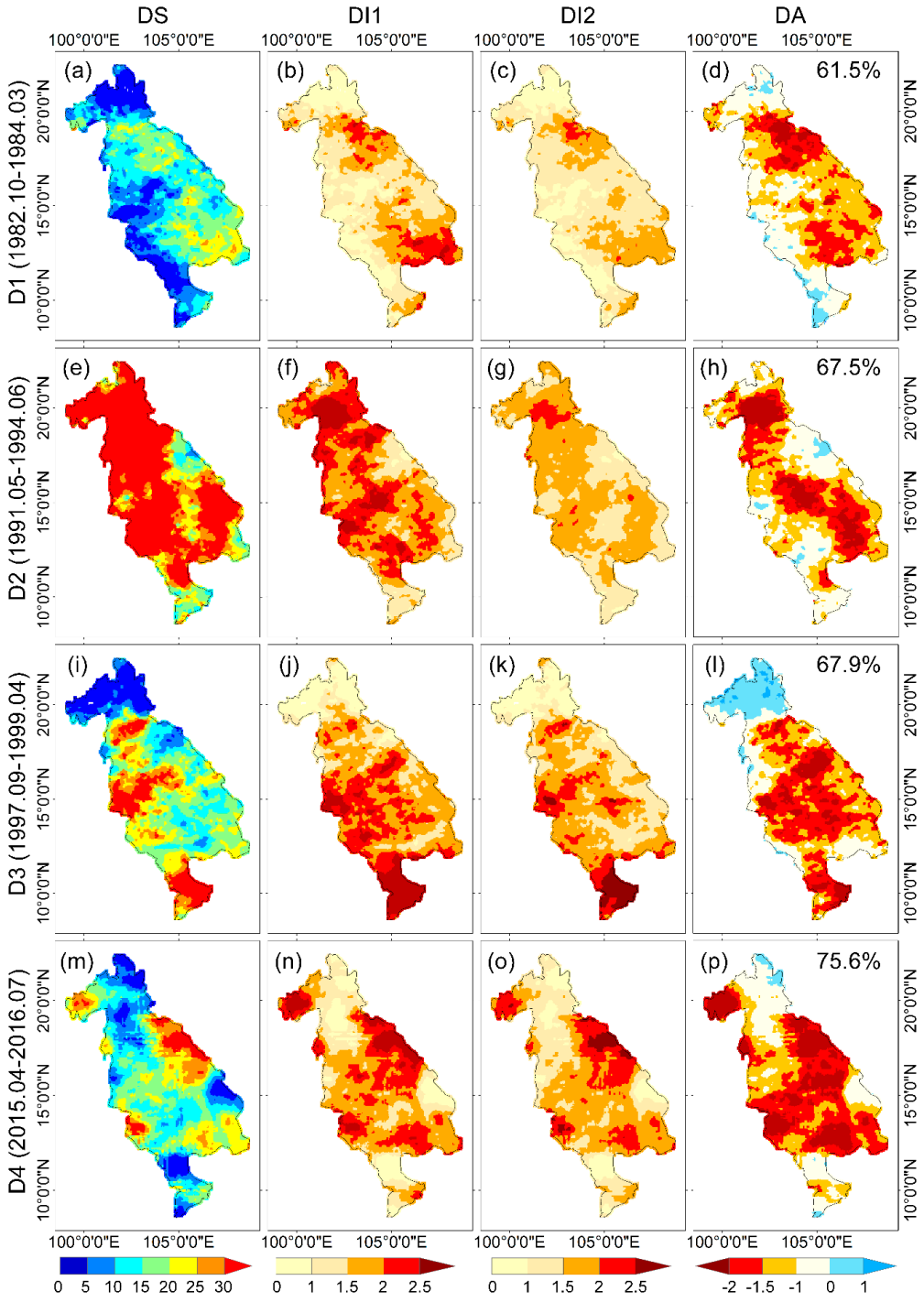

Figure 10. Spatial distribution of drought severity (DS), drought intensity (DI1 and DI2) and SPI value for the month with maximum drought area (DA) for four most severe drought events over LMB from 1981 to 2016: (**a**–**d**) D1, (**e**–**h**) D2, (**i**–**l**) D3 and (**m**–**p**) D4. All the statistics are based on SPI12.

3.3. Drought Impacts on Vegetation

The drought characteristics could help to understand the vegetation vulnerability to droughts, conversely, the vegetation response also can be helpful to assess the accuracy of drought monitoring by using CHIRPS. It should be noted that vegetation can only be used as a surrogate for drought monitoring when there are no artificial means introducing water to the plants, as vegetation could thrive even during a drought with timing irrigation. Here, the spatial averaged SAI_VHI and SPI3 are compared in Figure 11. It is well observed that SAI_VHI and SPI3 have a relatively agreeable evolution with a correlation coefficient value of 0.45. Though the correlation coefficient value is not very high, the variation of SAI_VHI generally corresponds well to the drought conditions with negative (positive) SAI_VHI value for dry (wet) periods. It is indicated that the meteorological droughts have great impacts on vegetation health. Conversely, the corresponding variation between the vegetation health condition and drought condition also indirectly reflect the fair capability of CHIRPS for drought monitoring in LMB region.

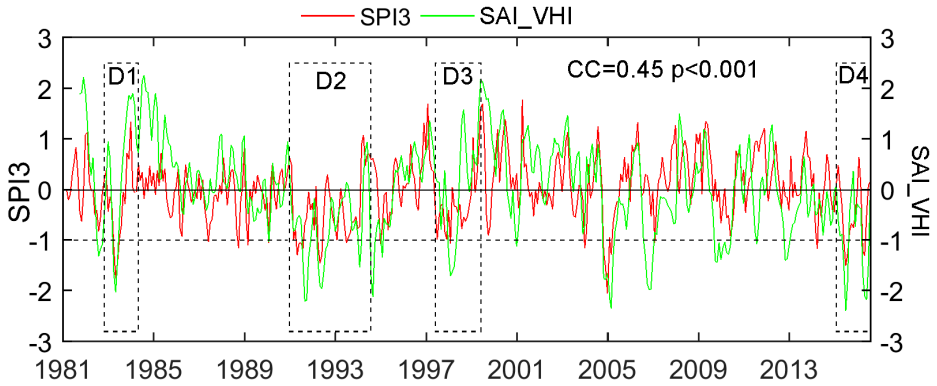

Figure 11. Time series spatial averaged SPI3 and SAI_VHI from 1981 to 2016. The four most severe drought events are marked by scattered rectangles.

Specifically, the relationship between region averaged SAI_VHI, SPI value and drought area at three-month scale during four drought periods are also compared and shown in Figure 12. The corresponding periods have also been marked by scattered rectangles and labels (D1, D2, D3 and D4) in Figure 11. The spatial averaged SPI and drought area at three-month time scale for the four drought events show that the four drought events have different drought evolutions with different drought intensity, drought severity and different drought duration. For example, D1 has only one drought area peek with corresponding lowest SPI value. D4 has two drought area peaks while D2 has variable drought area evolution with four drought area peaks. D3 has continuous mild drought area evolution with small fluctuation. The four distinctive drought events could help us to thoroughly test the drought impacts on vegetation and indirectly reflect the accuracy of the CHIRPS for drought monitoring.

As can be obviously observed in Figure 12, the SAI_VHI exhibit identical consistency with drought area for four much different drought events. For the short-term drought event (D1) with one drought peak, SAI_VHI also responds with one valley. When the drought area reaches a peak with lowest SPI value in April 1983, SAI_VHI value drops to the negative minimum. Moreover, SAI_VHI also can respond well to the small variation of drought area, like the small drought area peak in December 1982 and September 1983, as well as the relatively wet period from October to December 1983. Comparison with other drought events (D2, D3 and D4) shows good matches between the temporal variation of SAI_VHI and drought area. Quantitatively, there are some differences between the domain-averaged SPI3 and SAI_VHI values. The reasons for this difference can be complex, such as the influence of irrigation, the drought resistance of plants with different root system, the possible near-surface aquifer and the spatially averaged process of SPI. Overall, the above results suggest that the vegetation health is sensitive to the drought condition; in other words, the droughts have great impacts on

vegetation health condition. The results could also be indirect proof for the capability of CHIRPS for drought monitoring.

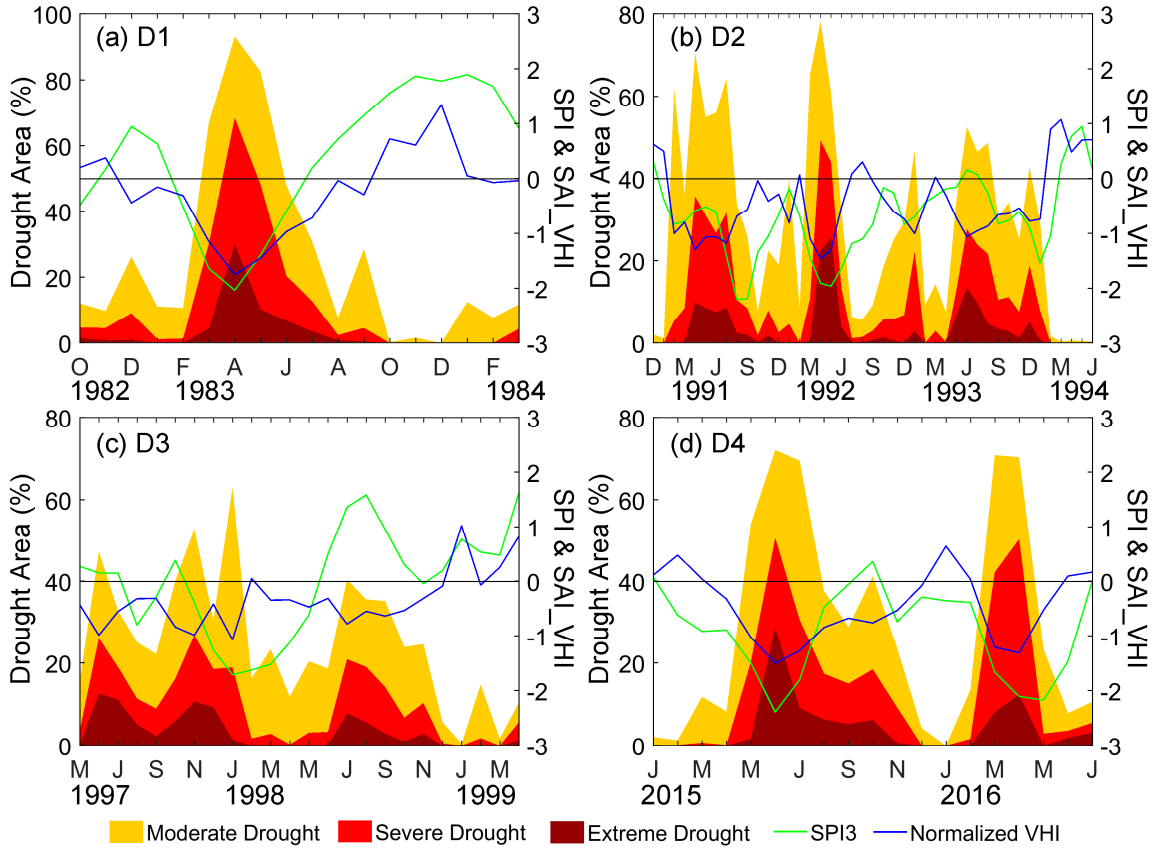

Figure 12. The relationship between SAI_VHI and drought indicators (SPI3 and drought area) during four specific drought events: (**a**) D1, (**b**) D2, (**c**) D3 and (**d**) D4. The events are also marked in Figure 11 by scattered rectangles.

4. Conclusions

LMB experiences concurrent drought events. The representativeness problem of rain gauges greatly limits the study of drought characteristics at the local scale. Availability of the latest monthly, 0.05° satellite-based CHIRPS provides an opportunity for long-term assessments of droughts at a finer resolution than previously possible. Based on a comparison of precipitation and SPI between CHIRPS and observed values, this paper focuses on monitoring drought conditions in Lower Mekong Basin from January 1981 to July 2016 using CHIRPS, which has a 36-year record of data. Two groups of rain gauges with different availability periods (20 gauges for the period of 1981–2016 and 38 gauges for the period of 1999–2016) were used as the reference to validate the stability of CHIRPS. SPIs at four different time scales (i.e., SPI1, SPI3, SPI6, and SPI12) were used to evaluate the drought conditions over LMB. The main findings of this study are as follows:

(1) CHIRPS shows reasonable ability to identify and characterize drought events. In comparison to rain gauges, CHIRPS performs well in estimating both monthly precipitation with high CC (0.98) and low RMSE (<13 mm/month) and SPI at different timescales. The results of three-month SPI (SPI3) have the best agreements while the relatively worse performance was detected at 12-month (SPI12) with slight overestimation in comparison with gauges. The SPI values at three-month timescale also exhibit high consistency with the variation of SAI_SM for the drought evolution.

(2) In the period of January 1981–July 2016, LMB experienced several severe drought events such as November 1982–February 1984, June 1991–May 1994, September 1997–April 1999, and April 2015—July 2016. The drought event from May 1991 to June 1994 is found as the longest one with drought duration of 38 months, and the drought of 2015–2016 is the most intense one with the lowest SPI value (−1.45), the highest averaged drought severity (0.97) and the largest drought affected area (75.6%).

(3) The total drought duration analysis further reveals that droughts occurred more frequently in the northern and southern LMB. Southwestern part of LMB and Mekong Delta region are more susceptible to severe drought events with long-term durations.

(4) The comparison between SAI_VHI and SPI3 shows that vegetation health is greatly influenced by droughts in LMB.

This study has demonstrated that CHIRPS is a valuable dataset for drought monitoring in Lower Mekong Basin. Results showed that the SPI derived from CHIRPS could detect drought events well by describing their temporal evolution, occurrence, and spatial distribution. Based on the advantage of high-resolution and long-term records of CHIRPS, it is found that four severe droughts occurred in Lower Mekong Basin with the longest one during 1991–1994 and the most intense one during 2015–2016 with drought affected area up to 75.6%. The analysis shows that the southwestern LMB and Mekong Delta region are more drought sensitive than other regions, which may be helpful to farmers for agricultural planning and drought management. In addition, the recurring droughts could have great impacts on vegetation conditions in LMB. The results of this study could provide valuable information for the improvement of sustainable water resource management.

Acknowledgments: This work was jointly funded by the National Key Research and Development Program of China (2016YFA0601601) and One Thousand Youth Talents Plan of China (Xinjiang Project: Y374231001). H.G. was supported by a grant from the program of China Scholarships Council (201604910968) during his stay in Ghent University, Gent, Belgium.

Author Contributions: Anming Bao conceived and designed the framework of this study. Hao Guo and Tie Liu processed the data, and analyzed the results under the supervision of Daming He, Alishir Kurban and Philippe De Maeyer. Hao Guo wrote the paper with the help from Felix Ndayisaba and Philippe De Maeyer. All authors contributed to the final version of the manuscript by proofreading and bringing in constructive ideas.

Conflicts of Interest: The authors declare no conflict of interest.

References

1. Wilhite, D.A. Drought as a natural hazard: Concepts and definitions. *Drought A Glob. Assess.* **2000**, *1*, 3–18.
2. Heim, R.R. A review of twentieth-century drought indices used in the united states. *Bull. Am. Meteorol. Soc.* **2002**, *83*, 1149–1165.
3. Kao, S.C.; Govindaraju, R.S. A copula-based joint deficit index for droughts. *J. Hydrol.* **2010**, *380*, 121–134. [CrossRef]
4. Keyantash, J.; Dracup, J.A. The quantification of drought: An evaluation of drought indices. *Bull. Am. Meteorol. Soc.* **2002**, *83*, 1167–1180.
5. Adamson, P.; Bird, J. The mekong: A drought-prone tropical environment? *Water Resour. Dev.* **2010**, *26*, 579–594. [CrossRef]
6. McKee, T.B.; Doesken, N.J.; Kleist, J. The relationship of drought frequency and duration to time scales. In Proceedings of the Eighth Conference on Applied Climatology, Anaheim, CA, USA, 17–22 January 1993.
7. Edwards, D.C. *Characteristics of 20th Century Drought in the United States at Multiple Time Scales*; DTIC Document; Colorado State University: Fort Collins, CO, USA, 1997; No. 634.
8. Hayes, M.; Svoboda, M.; Wall, N.; Widhalm, M. The lincoln declaration on drought indices: Universal meteorological drought index recommended. *Bull. Am. Meteorol. Soc.* **2011**, *92*, 485–488. [CrossRef]
9. Seiler, R.A.; Hayes, M.; Bressan, L. Using the standardized precipitation index for flood risk monitoring. *Int. J. Climatol.* **2002**, *22*, 1365–1376. [CrossRef]
10. Lu, E. Determining the start, duration, and strength of flood and drought with daily precipitation: Rationale. *Geophys. Res. Lett.* **2009**, *36*, L12707. [CrossRef]

11. Hao, Z.; AghaKouchak, A. A nonparametric multivariate multi-index drought monitoring framework. *J. Hydrometeorol.* **2014**, *15*, 89–101. [CrossRef]
12. Cancelliere, A.; Di Mauro, G.; Bonaccorso, B.; Rossi, G. Drought forecasting using the standardized precipitation index. *Water Resour. Manag.* **2007**, *21*, 801–819. [CrossRef]
13. Thomas, T.; Nayak, P.C.; Ghosh, N.C. Spatiotemporal analysis of drought characteristics in the bundelkhand region of central india using the standardized precipitation index. *J. Hydrol. Eng.* **2015**, *20*, 05015004. [CrossRef]
14. Joshi, N.; Gupta, D.; Suryavanshi, S.; Adamowski, J.; Madramootoo, C.A. Analysis of trends and dominant periodicities in drought variables in india: A wavelet transform based approach. *Atmos. Res.* **2016**, *182*, 200–220. [CrossRef]
15. De Jesús, A.; Breña-Naranjo, J.A.; Pedrozo-Acuña, A.; Alcocer Yamanaka, V.H. The use of trmm 3b42 product for drought monitoring in mexico. *Water* **2016**, *8*, 325. [CrossRef]
16. He, Y.; Ye, J.Y.; Yang, X.Y. Analysis of the spatio-temporal patterns of dry and wet conditions in the huai river basin using the standardized precipitation index. *Atmos. Res.* **2015**, *166*, 120–128. [CrossRef]
17. Guo, H.; Bao, A.M.; Liu, T.; Chen, S.; Ndayisaba, F. Evaluation of persiann-cdr for meteorological drought monitoring over china. *Remote Sens.* **2016**, *8*, 379. [CrossRef]
18. Lloyd-Hughes, B.; Saunders, M.A. A drought climatology for europe. *Int. J. Climatol.* **2002**, *22*, 1571–1592. [CrossRef]
19. Miao, C.Y.; Ashouri, H.; Hsu, K.L.; Sorooshian, S.; Duan, Q.Y. Evaluation of the persiann-cdr daily rainfall estimates in capturing the behavior of extreme precipitation events over china. *J. Hydrometeorol.* **2015**, *16*, 1387–1396. [CrossRef]
20. Kaptue, A.T.; Hanan, N.P.; Prihodko, L.; Ramirez, J.A. Spatial and temporal characteristics of rainfall in africa: Summary statistics for temporal downscaling. *Water Resour. Res.* **2015**, *51*, 2668–2679. [CrossRef]
21. Naumann, G.; Barbosa, P.; Carrao, H.; Singleton, A.; Vogt, J. Monitoring drought conditions and their uncertainties in africa using trmm data. *J. Appl. Meteorol. Climatol.* **2012**, *51*, 1867–1874. [CrossRef]
22. Huffman, G.J.; Adler, R.F.; Bolvin, D.T.; Gu, G.J.; Nelkin, E.J.; Bowman, K.P.; Hong, Y.; Stocker, E.F.; Wolff, D.B. The trmm multisatellite precipitation analysis (tmpa): Quasi-global, multiyear, combined-sensor precipitation estimates at fine scales. *J. Hydrometeorol.* **2007**, *8*, 38–55. [CrossRef]
23. Joyce, R.J.; Janowiak, J.E.; Arkin, P.A.; Xie, P.P. Cmorph: A method that produces global precipitation estimates from passive microwave and infrared data at high spatial and temporal resolution. *J. Hydrometeorol.* **2004**, *5*, 487–503. [CrossRef]
24. Ushio, T.; Sasashige, K.; Kubota, T.; Shige, S.; Okamoto, K.; Aonashi, K.; Inoue, T.; Takahashi, N.; Iguchi, T.; Kachi, M.; et al. A kalman filter approach to the global satellite mapping of precipitation (gsmap) from combined passive microwave and infrared radiometric data. *J. Meteorol. Soc. Jpn.* **2009**, *87*, 137–151. [CrossRef]
25. Turk, J.; Mostovoy, G.; Anantharaj, V. The nrl-blend high resolution precipitation product and its application to land surface hydrology. In *Satellite Rainfall Applications for Surface Hydrology*; Gebremichael, M., Hossain, F., Eds.; Springer: Dordrecht, The Netherlands, 2010; pp. 85–104.
26. Hsu, K.L.; Gao, X.G.; Sorooshian, S.; Gupta, H.V. Precipitation estimation from remotely sensed information using artificial neural networks. *J. Appl. Meteorol.* **1997**, *36*, 1176–1190. [CrossRef]
27. Sorooshian, S.; Hsu, K.-L.; Gao, X.; Gupta, H.V.; Imam, B.; Braithwaite, D. Evaluation of persiann system satellite–based estimates of tropical rainfall. *Bull. Am. Meteorol. Soc.* **2000**, *81*, 2035–2046. [CrossRef]
28. Yong, B.; Chen, B.; Gourley, J.J.; Ren, L.; Hong, Y.; Chen, X.; Wang, W.; Chen, S.; Gong, L. Intercomparison of the version-6 and version-7 tmpa precipitation products over high and low latitudes basins with independent gauge networks: Is the newer version better in both real-time and post-real-time analysis for water resources and hydrologic extremes? *J. Hydrol.* **2014**, *508*, 77–87.
29. Xue, X.; Hong, Y.; Limaye, A.S.; Gourley, J.J.; Huffman, G.J.; Khan, S.I.; Dorji, C.; Chen, S. Statistical and hydrological evaluation of trmm-based multi-satellite precipitation analysis over the wangchu basin of bhutan: Are the latest satellite precipitation products 3b42v7 ready for use in ungauged basins? *J. Hydrol.* **2013**, *499*, 91–99. [CrossRef]
30. Stisen, S.; Sandholt, I. Evaluation of remote-sensing-based rainfall products through predictive capability in hydrological runoff modelling. *Hydrol. Process.* **2010**, *24*, 879–891. [CrossRef]

31. Tan, M.; Tan, K.; Chua, V.; Chan, N. Evaluation of trmm product for monitoring drought in the kelantan river basin, malaysia. *Water* **2017**, *9*, 57. [CrossRef]
32. Tao, H.; Fischer, T.; Zeng, Y.; Fraedrich, K. Evaluation of trmm 3b43 precipitation data for drought monitoring in jiangsu province, china. *Water* **2016**, *8*, 221. [CrossRef]
33. Burroughs, W. *Climate: Into the 21st Century*; Cambridge University Press: Cambridge, UK, 2003.
34. WMO. Standardized precipitation index user guide. In *WMO-No. 1090*; Svoboda, M., Ed.; WMO: Geneva, Switzerland, 2012.
35. Ashouri, H.; Hsu, K.L.; Sorooshian, S.; Braithwaite, D.K.; Knapp, K.R.; Cecil, L.D.; Nelson, B.R.; Prat, O.P. Persiann-cdr daily precipitation climate data record from multisatellite observations for hydrological and climate studies. *Bull. Am. Meteorol. Soc.* **2015**, *96*, 69–83. [CrossRef]
36. Funk, C.C.; Peterson, P.J.; Landsfeld, M.F.; Pedreros, D.H.; Verdin, J.P.; Rowland, J.D.; Romero, B.E.; Husak, G.J.; Michaelsen, J.C.; Verdin, A.P. A quasi-global precipitation time series for drought monitoring. *U.S. Geol. Surv. Data Ser.* **2014**, *832*.
37. Katsanos, D.; Retalis, A.; Michaelides, S. Validation of a high-resolution precipitation database (chirps) over cyprus for a 30-year period. *Atmos. Res.* **2016**, *169*, 459–464. [CrossRef]
38. Katsanos, D.; Retalis, A.; Tymvios, F.; Michaelides, S. Analysis of precipitation extremes based on satellite (chirps) and in situ dataset over cyprus. *Nat. Hazards* **2016**, *83*, 53–63. [CrossRef]
39. Tuo, Y.; Duan, Z.; Disse, M.; Chiogna, G. Evaluation of precipitation input for swat modeling in alpine catchment: A case study in the adige river basin (Italy). *Sci. Total Environ.* **2016**, *573*, 66–82. [CrossRef] [PubMed]
40. Zambrano, F.; Wardlow, B.; Tadesse, T.; Lillo-Saavedra, M.; Lagos, O. Evaluating satellite-derived long-term historical precipitation datasets for drought monitoring in chile. *Atmos. Res.* **2017**, *186*, 26–42. [CrossRef]
41. Hoang, L.; Lauri, H.; Kummu, M.; Koponen, J.; van Vliet, M.; Supit, I.; Leemans, R.; Kabat, P.; Ludwig, F. Mekong river flow and hydrological extremes under climate change. *Hydrol. Earth Syst. Sci.* **2015**, *12*, 11651–11687. [CrossRef]
42. Son, N.T.; Chen, C.F.; Chen, C.R.; Chang, L.Y.; Minh, V.Q. Monitoring agricultural drought in the lower mekong basin using modis ndvi and land surface temperature data. *Int. J. Appl. Earth Obs.* **2012**, *18*, 417–427. [CrossRef]
43. Zhang, B.H.; Zhang, L.; Guo, H.D.; Leinenkugel, P.; Zhou, Y.; Li, L.; Shen, Q. Drought impact on vegetation productivity in the lower mekong basin. *Int. J. Remote Sens.* **2014**, *35*, 2835–2856. [CrossRef]
44. Hundertmark, W. Building drought management capacity in the mekong river basin. *Irrig. Drain.* **2008**, *57*, 279–287. [CrossRef]
45. Gupta, A.; Liew, S.C. The mekong from satellite imagery: A quick look at a large river. *Geomorphology* **2007**, *85*, 259–274. [CrossRef]
46. Leinenkugel, P.; Kuenzer, C.; Dech, S. Comparison and enhancement of modis cloud mask products for southeast asia. *Int. J. Remote Sens.* **2013**, *34*, 2730–2748. [CrossRef]
47. National Climatic Data Center; National Oceanic and Atmospheric Administration. *Department of Commerce Global Surface Summary of the Day*; GSOD National Climatic Data Center: Asheville, NC, USA, 2011.
48. Rizzoli, A.; Hauffe, H.C.; Tagliapietra, V.; Neteler, M.; Rosa, R. Forest structure and roe deer abundance predict tick-borne encephalitis risk in italy. *PLoS ONE* **2009**, *4*, e4336. [CrossRef] [PubMed]
49. Dingman, S.L. Normal radio method. In *Physical Hydrology*; Waveland Press: Long Grove, IL, USA, 2015; p. 115.
50. Funk, C.; Peterson, P.; Landsfeld, M.; Pedreros, D.; Verdin, J.; Shukla, S.; Husak, G.; Rowland, J.; Harrison, L.; Hoell, A.; et al. The climate hazards infrared precipitation with stations—A new environmental record for monitoring extremes. *Sci. Data* **2015**, *2*, 150066. [CrossRef] [PubMed]
51. NOAA. Avhrr Vegetation Health Product. Available online: https://www.star.nesdis.noaa.gov/smcd/emb/vci/VH/vh_ftp.php (accessed on 20 September 2016).
52. Bokusheva, R.; Kogan, F.; Vitkovskaya, I.; Conradt, S.; Batyrbayeva, M. Satellite-based vegetation health indices as a criteria for insuring against drought-related yield losses. *Agric. For. Meteorol.* **2016**, *220*, 200–206. [CrossRef]
53. Sholihah, R.I.; Trisasongko, B.H.; Shiddiq, D.; Iman, L.O.S.; Kusdaryanto, S.; Manijo; Panuju, D.R. Identification of agricultural drought extent based on vegetation health indices of landsat data: Case of subang and karawang, indonesia. *Proced. Environ. Sci.* **2016**, *33*, 14–20. [CrossRef]

54. Kogan, F.; Salazar, L.; Roytman, L. Forecasting crop production using satellite-based vegetation health indices in kansas, USA. *Int. J. Remote Sens.* **2012**, *33*, 2798–2814. [CrossRef]
55. Choi, M.; Jacobs, J.M.; Anderson, M.C.; Bosch, D.D. Evaluation of drought indices via remotely sensed data with hydrological variables. *J. Hydrol.* **2013**, *476*, 265–273. [CrossRef]
56. Mukherjee, T.; Mukherjee, S.; Mukhopadhaya, A.; Roy, A.K.; Dutta, S. Drought monitoring of chhattisgarh using different indices based on remote sensing data. In *Climate Change and Biodiversity: Proceedings of IGU Rohtak Conference, Vol. 1*; Singh, M., Singh, R.B., Hassan, M.I., Eds.; Springer: Tokyo, Japan, 2014; pp. 85–101.
57. DISC, G. Goddard Earth Sciences Data and Information Services Center. Available online: https://disc.sci.gsfc.nasa.gov (accessed on 21 September 2016).
58. Bordi, I.; Sutera, A. Drought monitoring and forecasting at large scale. In *Methods and Tools for Drought Analysis and Management*; Rossi, G., Vega, T., Bonaccorso, B., Eds.; Springer: Dordrecht, The Netherlands, 2007; Volume 62, pp. 3–27.
59. Sternberg, T.; Thomas, D.; Middleton, N. Drought dynamics on the mongolian steppe, 1970–2006. *Int. J. Climatol.* **2011**, *31*, 1823–1830. [CrossRef]
60. Ashraf, M.; Routray, J.K. Spatio-temporal characteristics of precipitation and drought in balochistan province, pakistan. *Nat. Hazards* **2015**, *77*, 229–254. [CrossRef]
61. Program to Calculate Standardized Precipitation Index. Available online: http://drought.unl.edu/MonitoringTools/DownloadableSPIProgram.aspx (accessed on 21 September 2016).
62. Yevjevich, V.M. *An Objective Approach to Definitions and Investigations of Continental Hydrologic Droughts*; Hydrology Papers; Colorado State University: Fort Collins, CO, USA, 1967.
63. Spinoni, J.; Naumann, G.; Carrao, H.; Barbosa, P.; Vogt, J. World drought frequency, duration, and severity for 1951–2010. *Int. J. Climatol.* **2014**, *34*, 2792–2804. [CrossRef]
64. Tan, C.; Yang, J.; Li, M. Temporal-spatial variation of drought indicated by spi and spei in ningxia hui autonomous region, china. *Atmosphere* **2015**, *6*, 1399–1421. [CrossRef]
65. Guo, H.; Chen, S.; Bao, A.M.; Hu, J.J.; Gebregiorgis, A.S.; Xue, X.W.; Zhang, X.H. Inter-comparison of high-resolution satellite precipitation products over central asia. *Remote Sens.* **2015**, *7*, 7181–7211. [CrossRef]
66. Tian, Y.D.; Peters-Lidard, C.D.; Choudhury, B.J.; Garcia, M. Multitemporal analysis of trmm-based satellite precipitation products for land data assimilation applications. *J. Hydrometeorol.* **2007**, *8*, 1165–1183. [CrossRef]
67. Sonmez, F.K.; Komuscu, A.U.; Erkan, A.; Turgu, E. An analysis of spatial and temporal dimension of drought vulnerability in turkey using the standardized precipitation index. *Nat. Hazards* **2005**, *35*, 243–264. [CrossRef]
68. Andreadis, K.M.; Clark, E.A.; Wood, A.W.; Hamlet, A.F.; Lettenmaier, D.P. Twentieth-century drought in the conterminous united states. *J. Hydrometeorol.* **2005**, *6*, 985–1001. [CrossRef]